View metadata, citation and similar papers at core.ac.uk
brought to you by CORE
provided by Kent Academic Repository

Multi-State Logging Freeze Detection Passive RFID Tags

M. Ali Ziai and John C. Batchelor, *Senior Member, IEEE*

***Abstract*—In this paper, the design and measurement of a passive UHF RFID smart tag suitable for monitoring and recording critical temperature violations in cold chain management are presented. The tag uses moving parts to detect and log different temperate states without the requirement for transceivers, memory, and batteries. A simple mechanical method is proposed whereby a moving metallic plate is trapped in one of four possible positions by specific environmental temperatures whereby inducing a permanent state-based change in the passive RFID tag response. The latched product critical temperature violations can be monitored via the read power required to turn on the tag transponder chip, which differs in each state.**

***Index Terms*—Mechanical sensors, radio frequency identification, RFID tags, temperature sensors.**

I. Introduction

THE logistic chain for chilled food is complex and can involve time-critical product management over large distances between origin and final delivery. Produce may undergo processing on-route and may be stored chilled or deep frozen. Food regulations established in various countries have placed responsibility for ensuring product safety and quality on the producers, processors, and retailers [1]. Monitoring critical temperature violation is particularly important in the frozen food supply chain as it can vary by up to 35% from the set temperature according to pallet position within a container [2], and with at least 10% of perishable foods reported to spoil in transit [3], there is a strong need to monitor and record critical-temperature violations using sensing devices during transportation. Commercial wireless sensor products for cold chain monitoring such as active RFID [4], semi-active RFID [5], or ZigBee [6] are versatile but require electronics, including memory and battery supplies, which drives up the cost and size of the unit. As a consequence, the deployment of sensors at individual item level is not economically feasible and critical-temperature monitoring can only be performed at pallet level with the data often inferred from a finite number of sensor nodes at various points along the route. As an alternative, ultra-high frequency (UHF) RFID tagging offers the potential to produce passive sensing systems with unit cost sufficiently low for item-level tagging if they are fabricated using new additive manufacturing processes, such as inkjet [7]. Such passive UHF RFID tags comprise a low-cost wireless transponder microchip connected directly to an etched, punched, or printed antenna on a low-cost, low-permittivity dielectric substrate.

Freeze/defrost sensing tags have been proposed [8] where a metal plate suspended in low-temperature aqueous-medium-filled cuboidal shell moves in close proximity of two RFID tag inlays positioned 3–5 cm apart on the outer surface of the sensor. The proposed sensor is required to be kept at below melting temperature prior to application, and once thawed, the metal plate is able to return to the initial position if the sensor or product position is oriented appropriately.

Recent work has presented the concept of a tag with mechanically moving parts to achieve accurate measurement of displacement [9]. Here, we propose a passive RFID tag sensor with four mechanically defined temperature sensing states to simplify calibration in the reading process and to reduce the potential for read errors. The tag sensing states exist sequentially and can only progress in one direction, meaning that the existence in one state implies the preceding states have already been experienced. The sensed states are as follows: one room/chill temperature (in the processing plant); two deep freeze (postprocessing and transit); three defrost (during transit); and four refreeze (predelivery).

The paper outlines the design of the mechanical-state-based tag system in Section II and describes the principle of sensing in Section III. The tag antenna design is provided in Section IV, and the effect of the mechanical system on the tag matching is shown. Measured results are presented in Section V, and Section VI concludes the paper.

II. Tag Design

The tag uses a moving plate to actuate the four states and comprises four parts, as shown in Fig. 1. With the exception of the tag antenna and the moving plate, all parts were fabricated from a rigid polymer (PTFE).

Referring to the elements depicted in Fig. 1, Part 1 is an $80 \times 50 \times 8$ mm^3 rectangular PTFE block, containing six small cylindrical reservoirs (8 mm diameter by 7 mm height). Each reservoir is connected to the block surface by a 2-mm-diameter nozzle, which, in turn, is covered by a thin flexible membrane. This surface also contains structures that constrain and guide a moving metal plate. Part 2 is a PTFE sheet that fits over the nozzle/membrane surface of Part 1 capturing the metal plate, which can freely move along a defined channel between the two parts. Part 3 is the tag antenna, etched in copper or printed by

Manuscript received May 09, 2014; revised August 29, 2014; accepted September 10, 2014. Date of publication September 19, 2014; date of current version November 25, 2014. This work was supported by the U.K. Engineering and Physical Sciences Research Council (EPSRC) under Grant EP/J000086/1.

The authors are with the School of Engineering, University of Kent, Canterbury, Kent, CT2 7HH, U.K. (e-mail: j.c.batchelor@kent.ac.uk).

Color versions of one or more of the figures in this paper are available online at http://ieeexplore.ieee.org.

Digital Object Identifier 10.1109/TAP.2014.2359474

This work is licensed under a Creative Commons Attribution 3.0 License. For more information, see http://creativecommons.org/licenses/by/3.0/

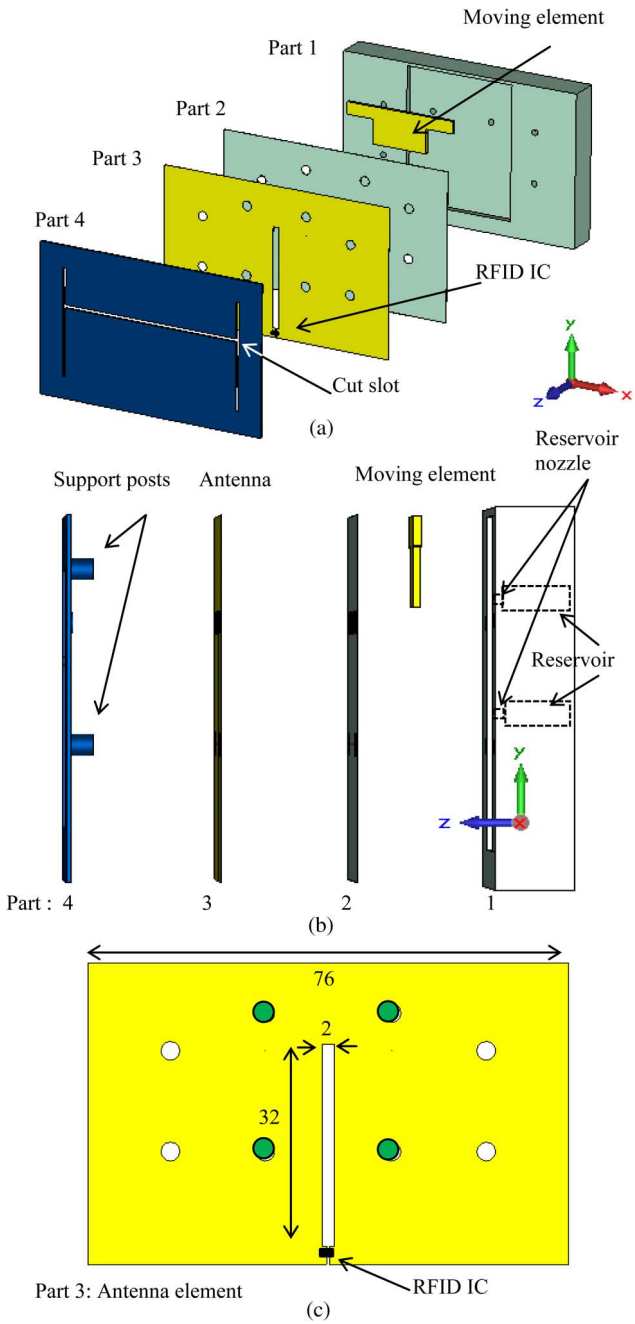

Fig. 1. (a) Exploded view of tag sensor parts; (b) side view; and (c) antenna; ● support guide post. All dimensions in millimeters.

some other means. Part 4 is a thin flexible polymer superstrate over the antenna, which acts to trap and release the metal plate within preset limits.

Before the parts were assembled, membranes were fitted over the reservoir nozzles. The metal plate was then placed between Parts 1 and 2 and the antenna attached, or potentially printed, onto Part 2. Finally, the reservoirs were filled with freeze point depressed water solution (i.e., an aqueous solution containing salt or alcohol, with a freezing point below 0 ℃). Conventional tooling processes were used for the prototype, but it is proposed to develop future tags using multiple material additive manufacturing techniques.

III. Sensor Principal of Operation

The existence in any individual state is indicated by the required transmit power produced by a reader to turn on the sensing tag and receive a response. This can be calibrated against a similar reference tag that is not sensitive to temperature and requires a turn-on power equal to state 1 of the sensing tag. The tag read range is obtained from [10] as

$$d \leq \lambda/4\pi\sqrt{\text{EIRP} \times G_{\text{tag}} \times \tau/P_{\text{th}}}, \tag{1}$$

where EIRP is the effective isotropic radiated power of the reader, G_{tag} is the tag antenna gain, τ is the power transmission coefficient between the tag antenna and the transponder chip, and P_{th} is the ASIC circuit activation threshold power. The tag antenna transmission coefficient τ is a function of sensed state, meaning the required EIRP to turn on the tag can be compared to that of the reference tag, which is an identical distance away, has the same transponder activation threshold power, and a known gain:

$$\frac{\text{EIRP}_n}{\text{EIRP}_{\text{Ref}}} = \frac{G_{\text{tagRef}}\tau_{\text{Ref}}}{G_{\text{tag}\_n}\tau_n} \tag{2}$$

where EIRP_n and EIRP_{Ref} refer to the reader-transmitted powers required to activate the sensing tag in State n, and the reference tag, respectively. G_{tag_n} and G_{tagRef} are the gain of the sensing tag in State n and the gain of the reference tag, respectively. τ_n and τ_{Ref} are the transmission coefficients of the sensing tag in State n and the reference tag, respectively.

The tag gain and transmission coefficient may be interdependent and are not easily separated in practice. However, the product of the two is a constant and known value for the reference tag, meaning the magnitude of the ratio on the right-hand side of (2) can be used to determine the sensed state in terms of τ, which is related to the reflection coefficient Γ of the tag antenna port referred to the chip input impedance [11]:

$$\tau = 1 - |\Gamma|^2 = \frac{4R_{\text{ic}}R_{\text{ant}}}{|Z_{\text{ic}} + Z_{\text{ant}}|^2} \tag{3}$$

where R_{ic} and R_{ant}, respectively, are the real parts of the respective transponder chip and antenna input impedances Z_{ic} and Z_{ant}. Therefore, the smart tag read range is directly related to the antenna impedance match. This principle is applied to sense the various states of the product critical temperature with quantized tag turn-on powers.

The state impedances are facilitated by the interaction between the slotline input impedance transformer of the antenna and the metal plate beneath. The plate moves in the cavity between parts 1 and 2, as shown in Fig. 2, and, in each of the four predetermined states, the plate position is limited by protuberances in the nozzle membranes and support pins fixed to part 4 (Fig. 1).

State 1 corresponds to the maximum read range of the sensing tag and occurs at room or chilled temperatures. In this state, the metal plate is restricted by the upper support posts for minimum interaction with the slot line and therefore has negligible effect on the antenna impedance.

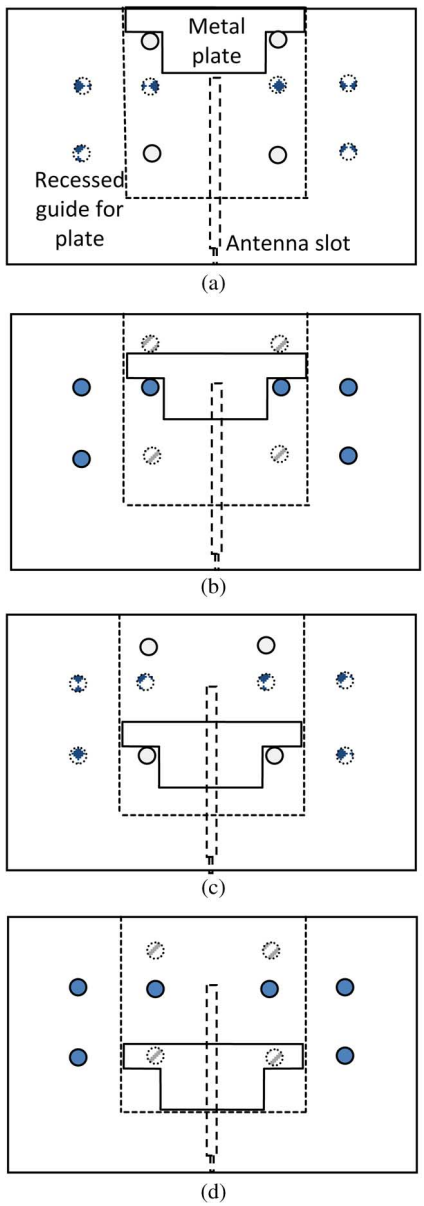

Fig. 2. Moving plate mechanism. State 1; (b) state 2; (c) state 3; (d) state 4. Nozzle: membrane protruding; membrane retracted. Support posts: supporting plate; retracted.

State 2 occurs as the temperature is lowered to deep freeze. The water solution trapped in the reservoirs freezes and expands, forcing the nozzle membranes to protrude outwards. This, in turn, displaces part 4, causing the support posts to move out of the path of the plate. The plate is released and moves freely under the force of gravity until stopped by the protruding membranes over the upper nozzles. In this position, the metal plate interaction with the slotline is increased, and the antenna impedance match degrades compared with state 1.

State 3 occurs if the temperature subsequently rises above the deep-freeze point. The water solution in the reservoirs melts, and the protruding membranes retract over the reservoir nozzles. The metal plate is released to drop further until stopped by the lower support posts. The plate impinges further on the antenna slot line, degrading the input match to a new level.

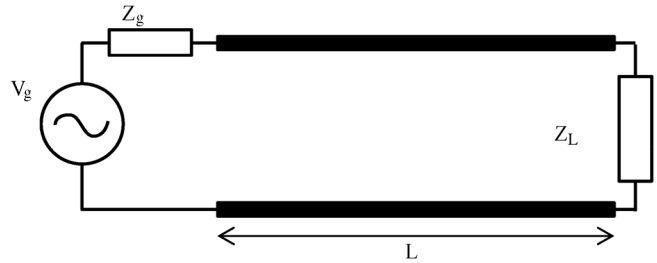

Fig. 3. Transmission line equivalent circuit of antenna slotline transformer.

Finally, state 4 exists when deep freeze recurs, causing the membranes to protrude, displacing the support posts, and releasing the metal plate to drop to position 4 at the bottom of the recessed guide. This results in the highest impedance mismatch.

IV. Tag Antenna Design

A slot antenna concept was chosen for the tag to achieve significant read range with little sensitivity to the mounting substrate, i.e. the frozen product. The antenna was attached to one side of part 3 (Fig. 1) and consisted of a rectangular patch with a narrow slot cut in the metallization. The slot acts as a transformer and provides a conjugate match to the RFID transponder IC [10]. The transponder can be considered to be connected to a slot line terminated with a short circuit load, and Fig. 3 shows the equivalent circuit where the voltage source V_g and the capacitive impedance Z_g represent the transponder. The antenna inductive impedance $Z_{\rm IN}$ depends on the characteristic and load impedances Z_0 and Z_L, respectively. For maximum power transfer, the antenna port impedance should conjugally match the RFID IC impedance $Z_{\rm ic} = Z^*_{\rm IN}$, where [10]

$$Z_{\rm IN} = Z_0 \left\{ \frac{(Z_L \cos(\beta L) + jZ_0 \sin(\beta L))}{(Z_0 \cos(\beta L) + jZ_L \sin(\beta L))} \right\} \tag{4}$$

and the slot line characteristic impedance is calculated form [12].

Initial design using (4) and optimization with CST Microwave Studio indicated the antenna slot width W and length L to be 2 and 35.5 mm, respectively, in order to match a transponder chip with impedance $Z_{\rm ic}$ of 30–j219 Ω on a substrate of relative permittivity $\varepsilon_r = 3.5$ and height = 9 mm. The simulated surface current on the antenna is shown in Fig. 4(a), where the eight holes accommodating the posts or membranes can be seen to have minimal effect as the maximum current is in the vicinity of the slot. This current concentration around the slot causes there to be significant interaction with the plate as it slides beneath [Fig. 4(b) and (c)]. The simulated radiation patterns shown in Fig. 4 indicate the tag has a directivity of 2.1 dBi for all plate positions though the efficiency, and, hence, the tag gain changes with plate position and significantly reduces in states 3 and 4, as indicated in Table I.

The entire sensor structure was adjusted to identify four metal plate positions, as depicted in Fig. 4(a)–(d), which offer discrimination in input impedance. Table I gives the antenna input impedances and S_{11} values at the European RFID band (868 MHz) for each of the selected metal plate positions and a significant level of detuning is apparent in each state. The antenna input impedance reduces between states 1 and 2 and then increases

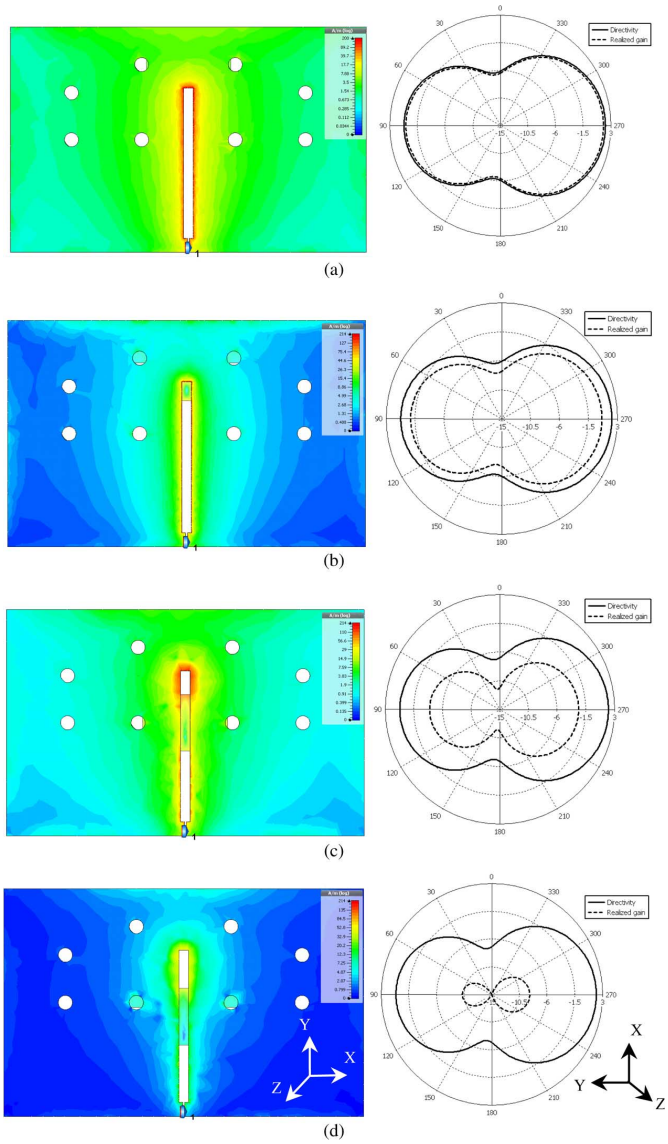

Fig. 4. Simulated current distributions and E-field radiation pattern (solid line = directivity, dashed line = realized gain) on antenna. State 1; (b) state 2; (c) state 3; and (d) state 4. —— Directivity; – – realized gain.

TABLE I
SIMULATED TAG PARAMETERS IN EACH SENSING STATE

State	Antenna Input Impedance (Ω)	*Antenna S_{11} Magnitude (dB)	Tag Total Efficiency (dB)	Gain (dBi)
1	22 + j220	-15.5	-0.2	1.9
2	16 + j192	-5.5	-2	0.2
3	104 + j426	-1	-7	-5.0
4	1130 +j790	-0.5	-11	-9.0

*Referred to transponder $Z_{IN} = 30 - j219\ \Omega$.

as the metal plate moves into states 3 and 4. This change of impedance is associated with the formation of an isolated hole at the top of the slot, which exists only for states 3 and 4 and significantly affects the current distribution.

The metal plate position also progressively affected the tag antenna overall efficiency and gain for Stages 1 to 4 as indicated in Table I. The directivity remained constant at 2 dBi and

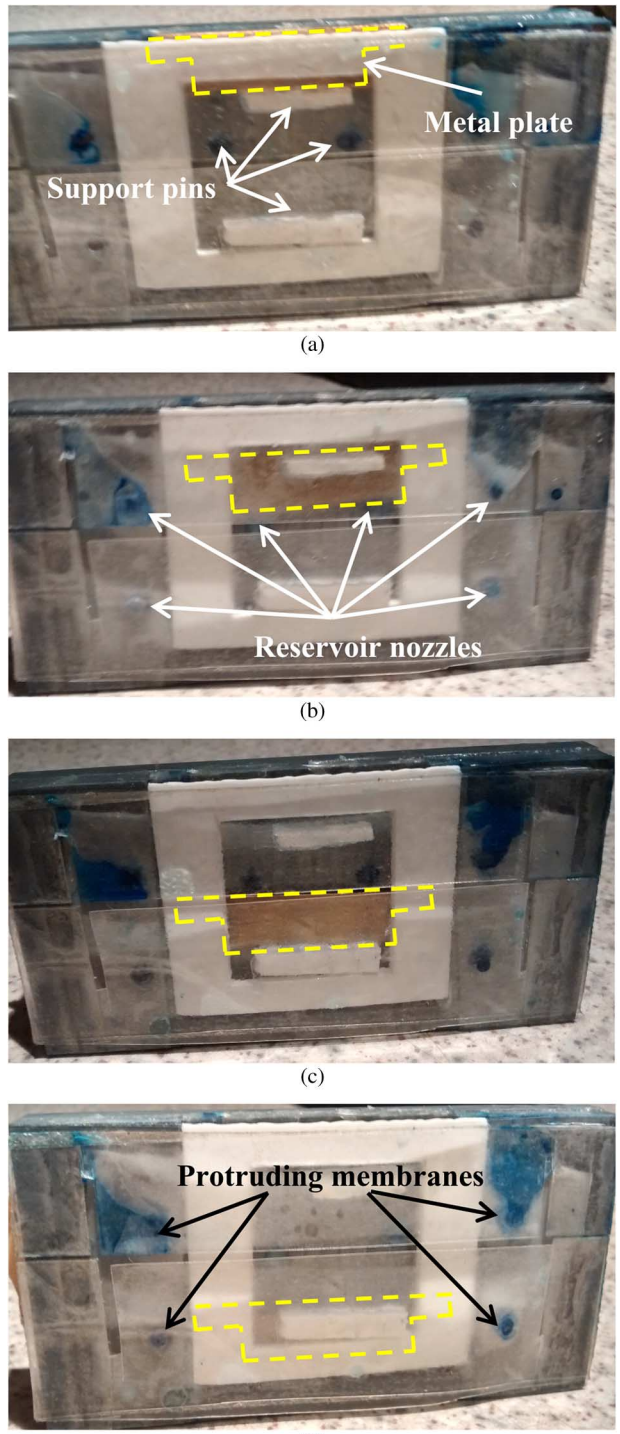

Fig. 5. Prototype sensor with antenna removed showing moving metal plate at (a) position 1 for room or chill storage temperature; (b) position 2 in deep freeze; (c) position 3 after defrost; and (d) position 4 after refreeze.

the gain reduction is caused by a falling in efficiency due to detuning by the metal plate as it moved closer to the antenna port as shown in Fig. 4.

V. MEASURED RESULTS

A prototype defrost sensing tag was fabricated to test the plate movement functionality. Fig. 5(a) depicts the assembled sensor with the antenna removed to show the initial plate position at

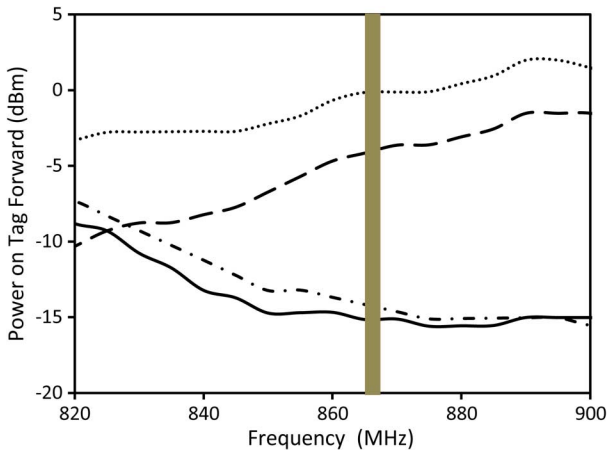

Fig. 6. Measured read range for four tag states. State 1: chilled; state 2: frozen; state 3: thawed; state 4: refrozen.

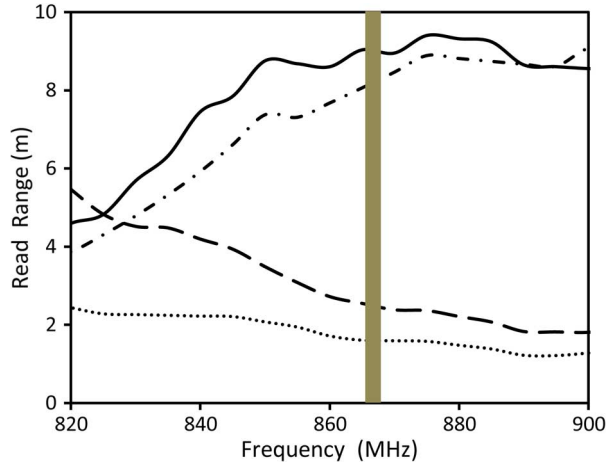

Fig. 7. Measured transmit powers required for tag turn-on in four tag states. State 1: chilled; state 2: frozen; state 3: thawed; and state 4: refrozen.

room temperature (20 ℃). The prototype was then placed in a freezer (−16 ℃) for 1 hour, and Fig. 5(b) illustrates how the metallic plate has dropped to position 2. This occurred as the water solution within the reservoirs froze, forcing the membranes over the nozzles to protrude. The metal plate was released from the first support pins allowing it to drop and rest on the protruding membranes. The prototype was then left at room temperature and, after 10 minutes, the water solution melted and retreated inside the reservoirs. This caused the plate to drop to position 3, as shown in Fig. 5(c). The final test was performed by replacing the prototype in the freezer for 1 hour. The membranes again protruded, pushing support block 3 outward and releasing the metal plate to drop into the lowest position, state 4, as shown in Fig. 5(d).

The sensing tag turn-on powers for each state were determined with a Voyantic Tagformance RFID characterization system [13], which uses a fixed transmission distance of one wavelength at 868 MHz to measure the backscattered powers for tags under test as a function of transmit power. The system is calibrated using a benchmark tag with a known response. The required turn-on powers and the maximum read ranges were found for each of the four states with the antenna attached to the sensing block and the metal plate in each of its positions. A clear discrimination can be observed between the four states in terms of read range (Fig. 6), with the largest distance being for state 1, which reduces by 0.4 m into state 2 to indicate a change from chilled to deep frozen. There is a clear fall of 5.5 m in read range to signal a defrost has occurred in state 3, with a further reduction of 0.9 m to indicate a refreezing in state 4.

Fig. 7 gives the required turn-on powers, which were measured at 868 MHz to be: state 1: −15 dBm, state 2: −14 dBm, state 3: −4 dBm, and state 4: 0 dBm.

From the simulated directivity and efficiency values in Table I, it is possible to calculate the required tag turn-on power in each state using (1) and (3), together with a transponder threshold value P_{th} of −15 dBm [14] and a factor incorporating path loss and other transmission losses that is chosen to agree with measurement. It can be seen in Fig. 8 that the simulated directivities and efficiencies offer close agreement

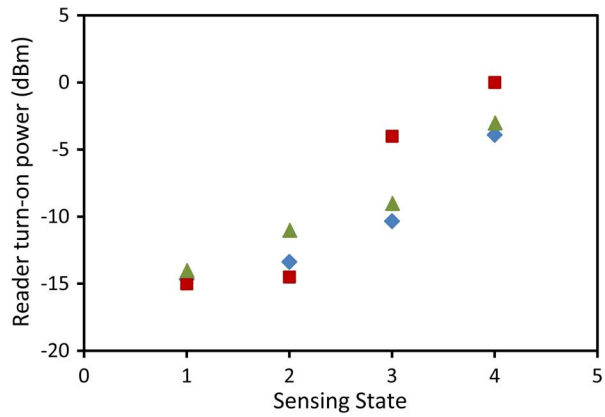

Fig. 8. Simulated and measured transmit powers required for tag turn-on in four tag states. ◆ Simulation; ■ measurement at 868 MHz; and ▲ measurement at 840 MHz.

to the measurements obtained from the Voyantic System at 868 MHz in states 1 and 2, while the calculated values are about 5 dB below those measured for states 3 and 4. Measurements at 840 MHz are also shown in Fig. 8 and better fit the calculations. The reason for the disagreement at 868 MHz is because the prototype tag was physically tuned to maximize the required turn-on powers in states 3 and 4 and making it slightly different from the simulated model.

VI. Conclusion

A passive, quantized state sensing tag with memory has been demonstrated by a machined prototype. The proposed design allows for simple calibration by using differentiated turn-on powers for four sequentially occurring states and straightforward comparison with non-sensing tags removes the need for acquiring information about tag orientation and channel characteristics. The increasingly large turn-on powers mean that, should refrigeration in the cold chain fail and the produce defrost, the tags will no longer be readable at several meters (states 3 and 4). A defrost/refreeze alert would arise if the tags must be brought within 1–2 m to read. Therefore, hand-held readers

may be used to identify the specific products which should be discarded.

Retuning of the tag should realize a greater distinction in turn-on power between the states, as for instance at 840 MHz, turn-on powers were measured to be -13, -11, -8, and -3 dBm for states 1 to 4, respectively. In industrial application, it may be appropriate to reduce the defrost/refreeze read ranges of states 3 and 4 to make is absolutely apparent that a defrost has occurred.

Future work will explore the potential of creating actuated state based sensing tags by additive manufacture which could reduce the overall tag thickness. In addition, performance in cold storage environments will be considered as well as the incorporation of a spring load on the plate to remove the need for gravity in the operation.

REFERENCES

[1] E. Abada, F. Palacio, M. Nuinc, A. González de Záratec, A. Juarros, J. M. Gómez, and S. Marco, "RFID smart tag for traceability and cold chain monitoring of foods: Demonstration in an intercontinental fresh fish logistic chain," *J. Food Eng.*, vol. 93, no. 4, pp. 394–399, 2009.

[2] D. Delen, B. C. Hardgrave, and R. Sharda, "The promise of RFID-based sensors in the perishables supply chain," Information Technology Research Inst., Univ. of Arkansas, Fayetteville, AR, USA, Aug. 2008 [Online]. Available: http://rfid.uark.edu/papers/ITRI-WP116-0808.pdf

[3] E. W. Schuster, S. J. Allen, and D. L. Brock, "Food: Dynamic expiration dates," in *Global RFID: The Value of the EPC Global Network for Supply Chain Management*. Berlin, Germany: GmbH, Springer-Verlag, 2007, pp. 127–134.

[4] Purelink Technology, Inc., 2012, SensorEdge, Temperature Sensor Tag, Product Data Sheet [Online]. Available: http://www.purelink.ca/en/Datasheets/PurelinkSensorEdge-PLK-SE030-TE1-TemperatureSensorTag.pdf

[5] CSL Convergence Systems Ltd., CS8300 Temperature Sensing Tag [Online]. Available: http://www.biltera.com.tr/rfidtaglist/isitakip/csl_cs8300.pdf

[6] *"XBee Drop-in Networking Accessories User's Guide"* [Online]. Available: http://ftp1.digi.com/support/documentation/90000891_G.pdf

[7] V. Sanchez-Romaguera, M. A. Ziai, D. O. Oyeka, S. Barbosa, J. S. R. Wheeler, J. C. Batchelor, E. A. Parker, and S. G. Yeates, "Towards inkjet-printed low cost passive UHF RFID skin mounted tattoo paper tags based on silver nanoparticle inks," *J. Mater. Chem. C*, vol. 1, no. 39, pp. 6395–6402, Aug. 2013.

[8] R. Bhattacharyya, C. Floerkemeier, and S. Sarma, "RFID tag antenna based temperature sensing," in *Proc. IEEE Int. Conf. RFID*, Orlando, FL, USA, 2010, pp. 8–15.

[9] C. Paggi, C. Occhiuzzi, and G. Marrocco, "Sub-millimeter displacement sensing by passive UHF RFID antennas," *IEEE Trans. Antennas Propag.*, vol. 62, no. 2, pp. 905–912, 2014.

[10] K. Finkenzeller, "Physical principles of RFID systems," in *RFID Handbook: Fundamentals and Applications in Contactless Smart Cards and Identification*, 3rd ed. New York, NY, USA: Wiley, 2010, pp. 61–154.

[11] K. V. S. Rao, P. V. Nikitin, and S. F. Lam, "Impedance matching concepts in RFID transponder design," in *Proc. 4th IEEE Workshop Autom. Ident. Adv. Technol. (AutoID 2005)*, Buffalo, NY, USA, 2005, pp. 39–42.

[12] K. C. Gupta, "Slotlines," in *Microstrip Lines and Slotlines*, 2nd ed. Norwood, MA, USA: Artech House, 1996, pp. 269–338.

[13] Tagformance: Measurement and Testing Solutions for the RFID Industry and Academia [Online]. Available: http://www.voyantic.com/tagformance

[14] C.-H. Loo, K. Elmahgoub, F. Yang, A. Elsherbeni, D. Kajfez, A. Kishk, and T. Elsherbeni, "Chip impedance matching for UHF RFID tag antenna design," *Progr. Electromagn. Res.* vol. 81, pp. 359–370, 2008 [Online]. Available: http://www.jpier.org/PIER/pier81/24.08011804.pdf

M. Ali Ziai received the M.Sc. degree in broadband and wireless communication engineering in 2008 and the Ph.D. degree from the University of Kent, Canterbury, U.K., in 2011.

He is currently employed as a Research Associate in the Antennas Group in the School of Engineering at the University of Kent. His main research activities are aimed at electrically thin and platform insensitive ultra high frequency radio frequency identification tags, especially for epidermal mounting and passive sensing.

John C. Batchelor (S'93–M'95–SM'07) received the B.Sc. and Ph.D. degrees from the University of Kent, Canterbury, U.K., in 1991 and 1995, respectively.

From 1994 to 1996, he was a Research Assistant with the Electronics Department, University of Kent, where he became a Lecturer of electronic engineering in 1997. He currently leads the Antennas Group at the University of Kent and is a Reader in Antenna Technology. His current research interests include UHF RFID tag design, passive sensing, body-centric antennas, printed antennas, compact multiband antennas, electromagnetic bandgap structures, and long-wavelength FSS (frequency-selective surfaces).